OBSERVATIONS OF THE VELOCITY FIELD OF NGC 4051[1]

NOBORU KANEKO

Department of Physics, Faculty of Science, Hokkaido University, Sapporo 060, Japan
Electronic mail: kanekon@s1.hines.hokudai.ac.jp

KENTARO AOKI,[2] GEORGE KOSUGI,[3] AND HIROSHI OHTANI

Department of Astronomy, Faculty of Science, Kyoto University, Kyoto 606-01, Japan
Electronic mail: aokikn@cc.nao.ac.jp; george@optik.mtk.nao.ac.jp; ohtani@kusastro.kyoto-u.ac.jp

MICHITOSHI YOSHIDA

Okayama Astrophysical Observatory, National Astronomical Observatory, Kamogata, Okayama 719-02, Japan
Electronic mail: yoshida@oao.nao.ac.jp

KIYOTAKA TOYAMA

Hokkaido Information University, Ebetsu 069, Japan
Electronic mail: toyama@do-johodai.ac.jp

TETSUYA SATOH

Kuriyama High School, Kuriyama, Hokkaido 069-15, Japan
Electronic mail: tsatoh@sun.email.ne.jp

MINORU SASAKI

Shimonoseki City University, Shimonoseki, Yamaguchi 751, Japan
Electronic mail: H01367@sinet.ad.jp

Received 1996 July 22; revised 1997 April 14

ABSTRACT

Observations of the velocity field of the Seyfert galaxy NGC 4051 were made using 1.88 m reflector of Okayama Astrophysical Observatory. For 106 H II and nuclear regions in 17 long-slit spectra (P.A. $=110°$) which covered almost an entire optical image of $\sim 3' \times 3'$, we measured Hα to present the velocities in tabular form. The emission region is rather annular, and the observed Hα velocities are gradually increasing with distance from the center to a radius of $\sim 90''$ with no maximum or flat part. Analyses give $V_h = 697 \pm 11$ km s^{-1} and $\phi = 130° \pm 14°$ for the heliocentric systemic velocity and the major axis position angle, respectively. Comparison shows that the Hα velocity structure is consistent with the H I observations of Liszt & Dickey (1995, AJ, 110, 998). However, the rotation curve corrected for the galaxy inclination ($i = 37°$) is different from any of the synthetic rotation curves of Rubin *et al.* (1985, ApJ, 289, 81) both in the form of rotation curve and in the absolute magnitude of galaxies. © *1997 American Astronomical Society.* [S0004-6256(97)03207-X]

1. INTRODUCTION

NGC 4051 is the closest known Seyfert 1 galaxy classified as a Sbc(r)II (Sandage & Tammann 1981) or SAB(rs)bc (de Vaucouleurs & de Vaucouleurs 1968) spiral. The excellent photographs of NGC 4051 have been published by Sandage & Bedke (1988, 1994). Their appearance shows that the barlike feature is prominent, extending up to $r \sim 50''$ along P.A. $\approx 130°$, and east and west spirals emanate from its both sides. Lots of knots are located on the spiral arms (Evans *et al.* 1996), and dust features are also prominent. Spiral features of NGC 4051 are asymmetric: the east spiral is extended to the northeast, while the west spiral appears possibly cutoff on the south by the dust extinction. The nucleus is not luminous in optical ($M_B = -15.2$, de Vaucouleurs & de Vaucouleurs 1968), but active in X-rays (Lawrence *et al.* 1985; Kunieda *et al.* 1992; McHardy *et al.* 1995; Papadakis & Lawrence 1995). Christopoulou *et al.* (1997) have recently published narrow-band imaging, long-slit spectroscopy, and MERLIN observations of the nuclear region of NGC 4051.

Together with its proximity ($d \approx 10$ Mpc for $H_0 = 75$ km s^{-1} Mpc^{-1}), moderate inclination ($i \approx 35° - 45°$) al-

[1]Based on observations made at Okayama Astrophysical Observatory (OAO). OAO is a branch of the National Astronomical Observatory, an inter-university research institute operated by the Ministry of Education, Science and Culture.
[2]Current address: National Astronomical Observatory, Mitaka, Tokyo 181, Japan.
[3]Current address: National Astronomical Observatory, Mitaka, Tokyo 181, Japan.

 0004-6256/97/114(1)/94/8/$10.00

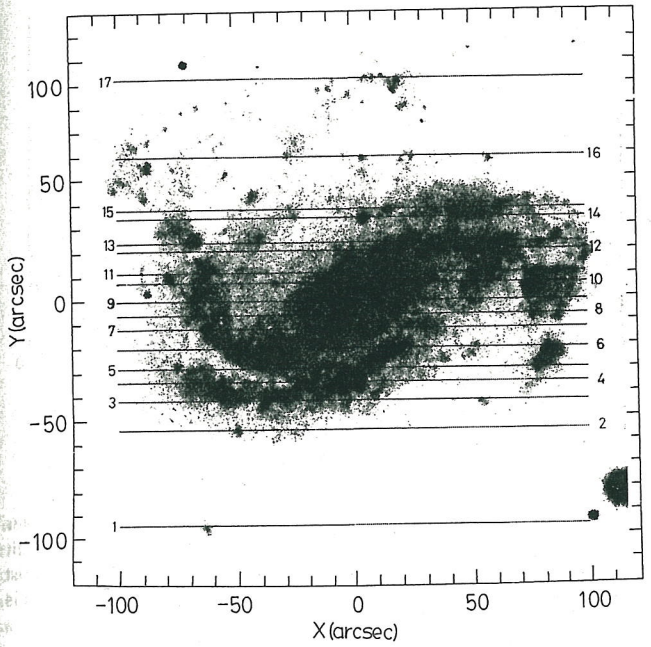

FIG. 1. Slit positions superposed on the B-band image of NGC 4051 reproduced from Sandage & Bedke (1988). The spectrograph slit was oriented at P.A.=110°, to which the x axis is parallel. The 17 slit positions are denoted by the figure. NNE is approximately up with ESE to the left.

lows a detailed study of the velocity field of the galaxy. As far as we know, however, no observations of the velocity field have been published for NGC 4051. The purpose of this paper is to present the observational data for the velocity field of NGC 4051.

2. OBSERVATIONS AND REDUCTIONS

The observations were made with the 1.88 m telescope at the Okayama Astrophysical Observatory in 1993 February 23–28. The telescope and the Cassegrain spectrograph were operated in the mode of Spectro-nebulagraph (SNG) (Kosugi *et al.* 1995), which is an area spectroscopic system to sweep automatically an object image with the slit. The SNG observations of active galaxies have been published for NGC 3516 by Aoki *et al.* (1994), NGC 5953 by Yoshida *et al.* (1993), and NGC 7319 by Aoki *et al.* (1996).

We set the slit (4.5′ in length and 1.8″ in width) to be in P.A.=110° so as to cover the H II regions effectively. Figure 1 shows the 17 slit positions overlaid on a B-band image reproduced from Sandage & Bedke (1988), where the (x,y) coordinate is a system with origin at the center of the galaxy, the x axis being parallel to the slit. In reading out the CCD, three pixels along the slit was binned, each pixel of resulting frames along the slit being 2.17″ on the sky.

Long slit spectra centered in the Hα region were obtained using a 600 grooves mm^{-1} grating blazed at 7500 Å. The dispersion is 1.2 Å (pixel)$^{-1}$ with a spectral resolution of 3.0 Å FWHM or 137 km s^{-1}. Exposure time was 1200 or 1800 s, and two frames were collected at each slit position. Similarly, Hβ−[O III] λλ 4959, 5007 spectra of brighter H II regions and the nucleus were obtained using a 600 grooves mm^{-1} grating blazed at 5000 Å, which are however insufficient in number to analyze the velocity field.

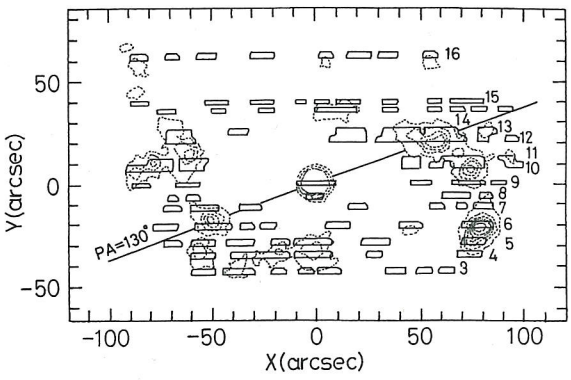

FIG. 2. The region from which each Hα spectrum is extracted and the Hα isophotes. P.A.=130° is the kinematic major axis position angle derived in this paper. The figure at the right indicates the slit number. The Hα image was obtained using the 60 cm Ritchey–Chretien telescope (F/8) at the Ouda Observatory, Kyoto University. Contour level is not calibrated, and higher isophotes are not shown at the nuclear region.

The comparison spectra of Ne and Fe were exposed between every successive exposures of the object. To monitor the drift of spectra along the slit, we obtained short-exposure nuclear spectra (180 or 300 s) once per about one hour. Flat frames were obtained by exposing the dome flat screen. The standard stars HD 19445 and HD 10995 (Barnes & Hayes 1982, 1984) were also observed.

The data reduction was performed using the IRAF[4] software package and SNGRED software package developed by two of us (G.K. and M.Y.). Bias subtraction, dark count subtraction, flat fielding, and removal of cosmic-ray events were carried out in a standard way. Wavelength calibration was made for each object frame using the two successive comparison spectra exposed before and after the object. Sky subtraction was made regarding regions off the galaxy as the sky background. The two successive short-exposure nuclear spectra were also used to correct for a small drift along the slit.

3. RESULTS

Figure 2 represents the regions from which Hα spectra are extracted, on which are superposed the contour map of the Hα image obtained using the 0.6 m Ritchey–Chretien telescope (F/8) at the Ouda Observatory, Kyoto University.

Examination of Fig. 2 reveals that Hα emission was not almost detected in the 90″×50″ central within which the stellar bar extending ~50″ in radius along P.A.≈130° is located. The spatial distribution of ionized gases in NGC 4051 is globally of an annular shape rather than a spiral pattern. However, this annular distribution does not originate from a single annular component in morphology. Comparison with the photograph in Fig. 1 and the Hα image of NGC 4051 recently published by Evans *et al.* (1996) shows that the emission knots in the southeast ($-60'' < x < 10''$, $-43''$

[4]IRAF is distributed by National Optical Astronomy Observatories, which is operated by the Association of Universities for Research in Astronomy, Inc. (AURA) under cooperative agreement with the National Science Foundation.

TABLE 1. Heliocentric Hα velocities of NGC 4051 (P.A.=110°).

Slit No.	y (arcsec)	$v(x)$ km s^{-1}			
1	−97.2	643±11 (−65.1)			
2	−54.5	518±21 (−51.0)			
3	−42.8	586±6 (−55.3)	598±5 (−38.0)	638±10 (−18.4)	645±7(−5.4)
		669±6 (5.4)	713±18 (36.9)	733±28 (51.0)	771±41 (61.8)
4	−34.7	587±4 (−55.3)	625±5 (−32.5)	645±4 (−17.4)	675±4 (−2.2)
		679±17 (27.1)	758±7 (72.7)		
5	−28.8	583±15 (−69.4)	600±4 (−55.3)	610±9 (−36.9)	658±5 (−17.4)
		680±5 (−7.6)	680±4 (2.2)	701±11 (28.2)	762±4 (74.9)
6	−20.9	558±7 (−72.7)	613±4 (−49.9)	643±17 (−33.6)	644±31 (−22.8)
		718±8 (9.8)	755±6 (44.4)	788±3 (77.0)	
7	−11.8	561±13 (−69.4)	604±6 (−54.2)	642±10(−31.4)	760±11 (19.5)
		764±21 (57.5)	783±27 (69.4)	786±9 (80.3)	
8	−6.2	584±14 (−69.4)	590±15 (−59.7)	704±30 (−1.1)	760±24 (64.0)
		787±22 (71.6)	803±9 (81.4)		
9	0.0	577±8 (−84.6)	604±6 (−61.8)	641±50 (−8.7)	644±13 (−6.5)
		637±7 (−4.3)	647±4 (−2.2)	658±4 (0.0)	668±4 (2.2)
		688±9 (4.3)	784±21 (49.9)	790±6 (72.7)	806±17 (87.9)
10	8.2	579±5 (−86.8)	587±4 (−74.9)	615±6 (−59.7)	777±14 (45.6)
		767±11 (57.5)	800±4 (72.7)	799±17 (95.4)	
11	12.0	592±4 (−74.9)	622±4 (−58.6)	774±8 (45.6)	792±7 (64.0)
		811±5 (74.9)	810±13 (92.2)		
12	21.7	606±5 (−65.1)	718±14 (9.8)	747±6 (19.5)	754±11 (31.4)
		781±4 (46.6)	803±4 (65.1)	811±16 (80.3)	819±16 (94.4)
13	25.7	610±6 (−66.2)	636±13 (−36.9)	738±8 (17.4)	771±4 (41.2)
		796±5 (54.2)	802±4 (62.9)	815±6 (82.4)	
14	36.0	616±13 (−71.6)	669±19 (−46.6)	682±12 (−22.8)	734±4 (9.8)
		779±14 (35.8)	783±23 (57.5)	816±14 (68.3)	822±20 (79.2)
		826±22 (92.2)			
15	40.0	626±18 (−84.6)	665±17 (−46.6)	695±14 (−24.9)	706±15 (−6.5)
		734±10 (3.2)	749±4 (16.3)	779±15 (35.8)	787±9 (57.5)
		795±8 (72.7)			
16	62.4	650±10 (−84.6)	660±40 (−68.3)	684±19 (−52.1)	689±11 (−25.0)
		722±9 (5.4)	747±9 (20.6)	789±19 (34.7)	795±7 (55.3)
17	96.3	726±12 (−6.5)	750±7 (7.6)	763±6 (16.3)	

Note – The figure in parentheses indicates the x coordinate in units of arcsec.

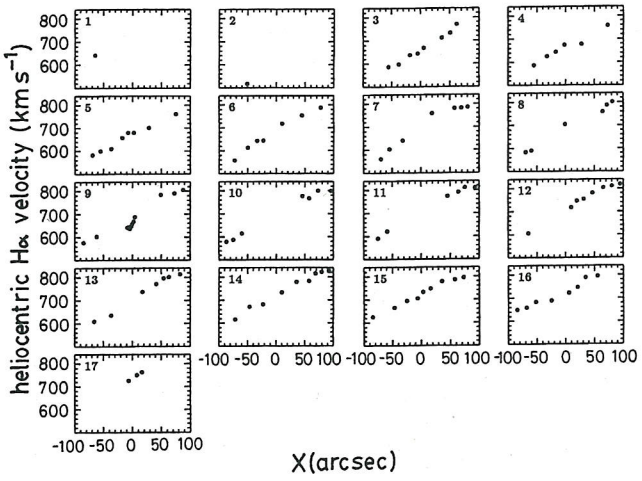

FIG. 3. Heliocentric Hα velocities as a function of distance from the center for NGC 4051. The figure at the upper left in each panel denotes the slit number. No maximum or flat part of the rotation velocities is found in most of the panels. In the nuclear region (panel 9), the gradient in the velocities is steeper than a rotation velocities inferred from a global velocity field.

$<y<-28''$) coincide well with a bow-like arm running parallel to a southeast portion of the stellar bar. On the other hand, an east portion of the annular distribution ($-90''<x<-50''$, $-21''<y<40''$) corresponds to the east spiral tangentially emanating from a southeast limit of the bar, and the upper knots are correspondent to diffuse spiral features asymmetrically extending to the north. In the southwest quadrant most emission comes from the knots lying on the disturbed west spiral.

The radial velocity was determined by fitting a Gaussian profile to each binned spectrum. In deblending the complex Hα+[N II] λ6548+λ6583, we assumed that each line width is the same within the blended complex and that the mutual separation of the central wavelengths is equal to the theoretical one. The intensity ratio of [N II] λ6583/λ6548 was fixed to the theoretical value 3.0. Similar assumptions were also made for [O III] λ4959+λ5007. The errors in the measurements of the velocities have been estimated to be of order or better than ± 15 km s^{-1} for moderate/strong lines and $\pm(30-50)$ km s^{-1} for weak lines.

We present all measured Hα velocities both in tabular and graphical forms. First and second columns of Table 1 list the slit-position number and the y coordinate (P.A.=20°), respectively. The figure in parentheses attached after the velocity indicates the x coordinate (P.A.=110°). The uncertainties listed in the table are standard errors of the mean. The velocities presented here are heliocentric. Velocities referred to in this paper are heliocentric. The correction to the Galactic Center is calculated to be $\Delta v=+52$ km s^{-1} following a simple solution of $\Delta v=300 \sin l \cos b$ (RC2; Tully 1988) or $\Delta v=+47$ km s^{-1} using equation (81) of RC3. We also have $\Delta v=+40$ km s^{-1} for the correction to the centroid of the Local Group (Yahil *et al.* 1977; RSA).

In Fig. 3 are plotted the Hα velocities as a function of x for the 17 slit positions. One of the features of Fig. 3 is that there appear no velocity structures to suggest a maximum or flat part of the rotation velocities. Except for two panels (No. 1 and No. 2) in which only one point of velocity is plotted and the nuclear velocities in the panel of No. 9, our observed Hα velocities show behaviors gradually varying along the slit. The other feature is that in the panel of No. 9 the velocity structure within ~10″ from the center is different from that outside ~10″ radius. This seems to suggest that the kinematic major axis rotates within the nuclear region. We have reported a similar velocity structure for NGC 1068 (Kaneko *et al.* 1992). No velocities within 8.″3 in radius are, therefore, taken into account in analyzing velocity structures.

To see a global velocity structure, we plot in Fig. 4 all Hα velocities as a function of x, where odots indicate the velocities at the nuclear region of No. 9. Open circles denote the velocities in the northeast (No. 17 and the left parts ($x<0$) of Nos. 14–16) and southwest (Nos. 1–2, and the right parts ($x>0$) of Nos. 3–5) regions. The figure attached to the open symbols is the slit number. As mentioned in the Introduction, the former corresponds to the region within which is included the east spiral asymmetrically extending to the north, while the latter is the region possibly affected by the dust extinction. Figure 4 appears to suggest a twist of the velocity field or a warp of the disk. As we are interested in the global velocity structure of NGC 4051, the velocities denoted by filled circles shall be analyzed in deriving the kinematic parameters of the galaxy.

In addition to the radial velocities, we tried to measure the [N II]/Hα intensity ratio for ~100 H II regions. The mean value is $\log I([\text{N II}])/I(\text{H}\alpha)=-0.43\pm0.14$. For five bright H II regions we also measured the intensity ratios of [O III]

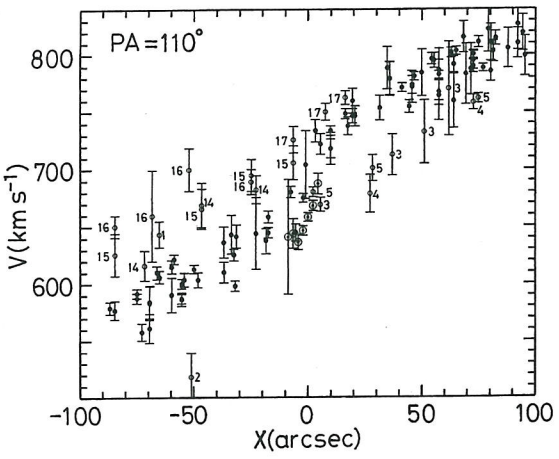

FIG. 4. Plots of all observed Hα velocities as a function of distance from the center for NGC 4051. Open circles denote the velocities at the following slit positions: No. 1, No. 2, and No. 17, the right parts ($x>0$) of Nos. 3–5, and the left parts ($x<0$) of Nos. 14–16. Odots indicate the velocities at the nuclear region. The figure attached to the open symbol is the slit number.

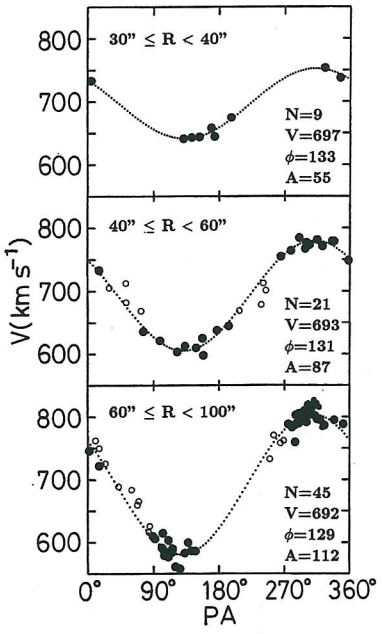

FIG. 5. Observed Hα velocities as a function of position angle. Small open circles correspond to the open symbol in Fig. 4, which are not included in the fitting. The velocities were fitted with a cosine curve, and the number of data N, the velocity V(km s^{-1}) corresponding to a systemic velocity, the major axis position angle ϕ(°), and the velocity amplitude A(km s^{-1}) are given for each velocity range. Fitting errors for the position angle and the systemic velocity are 18° and 8 km s^{-1} ($30''\leq R<40''$), 12° and 10 km s^{-1} ($40''\leq R<60''$), and 12° and 12 km s^{-1} ($60''\leq R<100''$). We adopt $\phi=130°\pm14°$ and $V_h=693\pm11$ km s^{-1} for the major axis position angle and the heliocentric systemic velocity, respectively.

λ5007/Hβ and [N II] λ6583/Hα to obtain log I([O III])/I(Hβ)≈(−0.78)−(−0.34) and log I([N II])/I(Hα)≈(−0.51)−(−0.42). These results imply that our spectra are of normal H II regions (Evans & Dopita 1985; Veilleux & Osterbrock 1987).

4. DISCUSSION

4.1 Major Axis, Systemic Velocity, and Galaxy Inclination

The kinematic parameters can, in principle, be determined simultaneously by applying the least squares method, provided that a form of the rotation law is assumed. However, as mentioned above, our observational data suggest that the rotation law of NGC 4051 increases with distance from the center with no maximum or flat part. Such a form of the rotation law is unsuitable to a simultaneous determination of the parameters (Kaneko *et al.* 1992).

For three radius ranges ($30''\leq r<40''$,$40''\leq r<60''$,$60''\leq r<100''$), we plot in Fig. 5 the Hα velocities as a function of position angle, where a fitted cosine curve, N the number of data used, V (km s^{-1}) the velocity corresponding to a systemic velocity, ϕ(°) the major axis position angle, and A (km s^{-1}) the velocity amplitude are given for each velocity range. Small open circles correspond to the velocities indicated by open circles in Fig. 4, which are not used in the least squares fitting. Although observed velocities do not cover the whole angle, the three sets of fitted parameters agree well with each other. The average of them gives $\phi=130°\pm14°$ for the major axis position angle, consistently with the morphology. We also have $V_h=693\pm11$ km s^{-1} for the heliocentric systemic velocity. According to the RC3, the major axis of NGC 4051 is $\phi=135°$, and its heliocentric optical and H I velocities are, respectively, V_h (opt) = 688 ± 13 km s^{-1} and V_h(H I) = 725 ± 5 km s^{-1}. V_h = 706 km s^{-1} is also given in the RSA as the weighted mean observed velocity of NGC 4051. According to Huchra & Burg (1992), the heliocentric velocity of NGC 4051 is V_h = 674 km s^{-1}.

The galaxy inclination was calculated from published axial ratios: $i=34°$ (Nilson 1973), $i=35°$ (Kodaira *et al.* 1990), $i=37°$ (Sandage & Bedke 1988), $i=40°$ (Simkin *et al.* 1980), and $i=44°$ (de Vaucouleurs & de Vaucouleurs 1968). The average of these five values gives $i=38°$, and except for a slightly larger value of $i=44°$, we have $i=37°$. In this paper, we adopt $i=37°$ as the inclination of the galaxy.

4.2 Velocity Structure and Rotation Curve

The velocity corrected for the galaxy inclination $V(R)$ is calculated using

$$V(R)=\frac{v(r,\theta)-V_h}{\sin i\,\cos(\theta-\phi)}\cdot\frac{R}{r}, \tag{1}$$

where (r,θ) is a polar coordinate system in the plane of the sky with common origin at the nucleus and with the angles measured from the north, ϕ is the position angle of the line of nodes, $v(r,\theta)$ is the observed velocity, and R the radius projected on the galaxy plane is given by

$$\frac{R}{r}=\frac{\sqrt{1-\sin^2 i\,\cos^2(\theta-\phi)}}{\cos i}. \tag{2}$$

The correction for the galaxy inclination of $i=37°$ was made using Eqs. (1) and (2). The result is shown in Fig. 6, where open and filled circles correspond to the velocities in the two half sides divided by the minor axis (P.A.=40°). Small symbols are the velocities denoted by open circles in

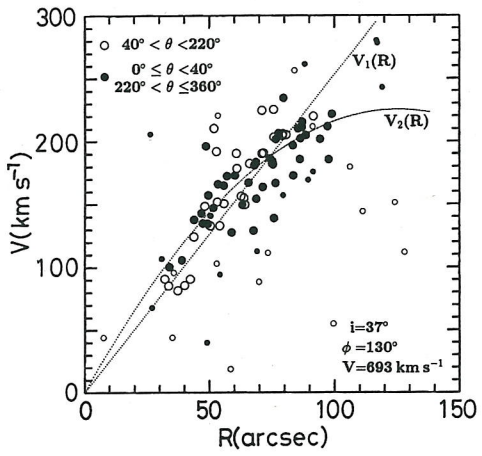

FIG. 6. Hα velocities corrected for the galaxy inclination. The parameters $i=37°$, $\phi=130°$, and $V_h=693$ km s^{-1} were used in the correction. Open and filled circles correspond to the velocities in the two half sides divided by the minor axis (P.A.=40°), and small symbols correspond to the open circle in Fig. 4, which are excluded in the fitting. If only circular motions occur, rotation velocities are negative in the approaching side ($40°<\theta<220°$), and positive in the receding side ($0°\leqslant\theta<40°$, $220°<\theta\leqslant360°$). The velocities were fitted with linear and quadratic equations, which are denoted by $V_1(R)$ and $V_2(R)$, respectively.

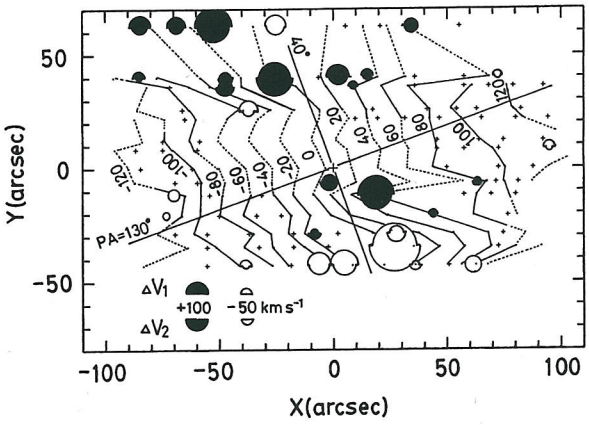

FIG. 7. Isovelocity contours and corrected velocity minus fitted rotation velocity. The contour interval is 20 km s^{-1}, and velocities are offsetted by 693 km s^{-1}. Upper half circles denote ΔV_1 the excess velocity from V_1 the rotation velocities fitted by the linear equation, and under half circles indicate ΔV_2 the excess from V_2 the rotation velocity estimated from the quadratic law. The data points having $|(\Delta V_1+\Delta V_2)|/2>30$ km s^{-1} are plotted in the diagram. Open and filled symbols represent the negative and positive excess velocities, respectively.

Fig. 4, which are not included in the following least-squares fitting. The velocities at the nuclear region are not plotted. If only circular motions occur, rotation velocities are negative in the approaching side ($40°<\theta<220°$), and positive in the receding side ($0°\leqslant\theta<40°$, $220°<\theta\leqslant360°$).

Except for the velocities denoted by small symbols, Fig. 6 reveals a shape of the rotation curve gradually increasing with distance from the center. The velocities were therefore fitted with linear and quadratic equations. For the resultant linear and quadratic equations, we have

$$V_1(R)=(2.53\pm0.31)R \text{ km s}^{-1}, \quad (3)$$

$$V_2(R)=(3.59\pm0.29)R-(0.0143\pm0.0038)R^2 \text{ km s}^{-1}, \quad (4)$$

where R is in units of arcsec. The least-squares fitting was also applied individually to the velocities both in the approaching and receding sides, since the open and filled circles appear to show slightly different slopes in the velocity curves. The result gives 2.69 ± 0.52 and 2.43 ± 0.39 as the coefficient of linear equation for the open and filled circles, respectively. Ignoring fitting errors, this yields a departure of ±12 km s^{-1} from Eq. (1) at $R=90''$. If quadratic equations are applied, ±16 km s^{-1} is obtained at $R=90''$ as the departure from Eq. (2). Thus, it is evident that the velocity field of NGC 4051 is asymmetric with respect to the minor axis (P.A.=40°). However, the above departures are smaller than the uncertainties in the fitting procedure. In this paper we are concerned with the rotation laws of Eqs. (1) and (2) as a global velocity field of NGC 4051.

The fitted rotation velocities of V_1 and V_2 were subtracted from the corrected velocities. The resultant excess velocities ΔV_1 and ΔV_2 give a measure for the departure from the fitted rotation law. Together with isovelocity contours, we plot in Fig. 7 the data points having $|(\Delta V_1+\Delta V_2)|/2>30$ km s^{-1}, where the upper and under half circles are correspondent to ΔV_1 and ΔV_2, respectively, and positive and negative excesses are also indicated by filled and open symbols, respectively.

Isovelocity contours are radial about the center for the case in which a rotation velocity is constant, and the contours are perpendicular to the line of nodes for the case in which the rotation velocity is proportional to the radius from the center. NGC 4051 is evidently the latter case, and the contours in Fig. 7 seem globally perpendicular to P.A.=130° the major axis position angle determined in the present paper. This is interpreted to mean that within a radius of ~90″ from the center the velocity structure of NGC 4051 is primarily of a rigid body rotation.

Furthermore, we can see in Fig. 7 that velocity departures from the circular motion are large especially in the northeast region corresponding to the open circles plotted in Fig. 4. Although this suggests a physical relation between the peculiar features in morphology and velocity departures from the circular motion, our present observations are unfortunately insufficient in spacing for further analyses of the nature of such noncircular motions.

4.3 Comparison with the H I Observations of Liszt & Dickey (1995)

Recently, Liszt & Dickey (1995) have published the H I observations of NGC 4051 made with the synthesized beamwidth of 37.8″. According to them, the galaxy has an annular H I distribution with a maximum H I surface density at $R\approx75''$, and the H I velocity field is rather regular and noncircular motion is negligible. They have derived V_h(H I) $=703$ km s^{-1} as the heliocentric systemic velocity and ϕ(H I) $=132°$ as the position angle for the line of node. These values are in good agreement with our results derived above. The H I data base of Bottinelli *et al.* (1990) give V_h(H I) $=725\pm4$ km s^{-1} for NGC 4051.

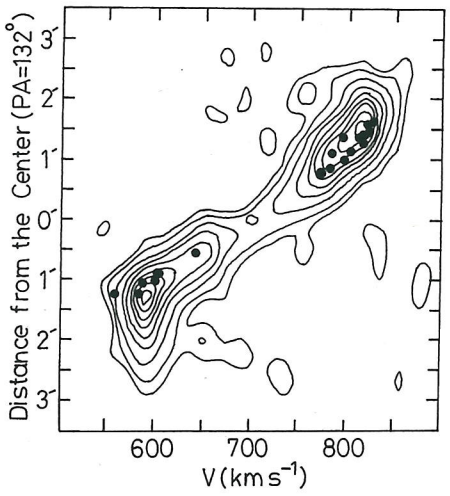

FIG. 8. Comparison with the H I velocity-position map of Liszt & Dickey (1995). Liszt & Dickey adopted P.A.=132° as the major axis position angle, and so, the Hα velocities within P.A.=132°±10° are plotted. The velocities at the nuclear region are not shown in the diagram.

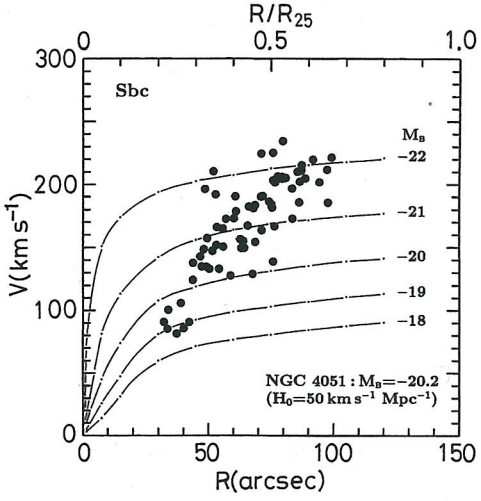

FIG. 9. Comparison with the synthetic rotation curves of Sbc spirals. The synthetic rotation curves of Sbc galaxies were calculated from a simple mean of the synthetic rotation curves compiled by Rubin *et al.* (1985) for Sb and Sc galaxies. NGC 4051 is classified as a Sbc spiral. Its absolute magnitude and isophotal radiusis are taken to be $M_B=-20.2$ ($H_0=50$ km s^{-1} Mpc^{-1}) and $R_{25}=150''$ (RC2), respectively. It should be noted that the rotation velocities of NGC 4051 are different from any of the Sbc synthetic rotation curves both in the form of the rotation curve and in the absolute magnitude of galaxies.

Figure 8 is the comparison with the H I velocity-position map (P.A.=132°) of Liszt & Dickey (1995), where we plot the optical velocities within the position angles of 132°±10° and 312°±10°. The velocities at the nuclear region are not plotted in the diagram. Examination of Fig. 8 reveals that within ~90″ from the center our optical velocities are consistent with the velocity structure of H I emission.

Liszt & Dickey (1995) show in their Fig. 7(a) that the H I rotation curve of NGC 4051 consists of rising inner part and nearly flat outer part. The flattening of the H I rotation curve is found to occur at $R\sim100''$, which is also nearly the outer boundary of the optical image of NGC 4051. This implies that the optical disk of NGC 4051 rotates following a simple rotation law, and the outer envelope or halo region with a nearly constant velocity. From Fig. 7(a) of Liszt & Dickey (1995), the velocity of the flat part is estimated to be $V_{\rm flat}({\rm H\,I})\sim180$ km s^{-1}, which is corrected for the galaxy inclination of $i=40°$. Then, we have $V_{\rm flat}({\rm H\,I})\sim193$ km s^{-1} after the correction for the inclination of $i=37°$ adopted in this paper. If the optical rotation curve of NGC 4051 has a shape similar to that of H I emission, we may guess $V_{\rm flat}({\rm H}\alpha)\sim200$ km s^{-1} from Fig. 6. NGC 4051 is evidently one of the galaxies characterized by a flat outer portion of the rotation curve.

It should be also noticed in Fig. 8 that a sharp bending structure corresponding to the flattening of the rotation curve is seen within the distance of ~1.5′–2.8′ from the center at $v\sim580$ km s^{-1}. Such a bending structure is weak at the northwest receding side, implying that, outside the optical disk of ~1.5′ in radius, H I emission has some irregularities both in intensity and velocity structures. The asymmetric spiral structure mentioned in the Introduction and large velocity departures from the circular motion shown in Fig. 7 may be possibly attributed to such irregular features. Here, it is interesting to note that Byrd *et al.* (1987) have suggested a tidal interaction with an edge-on Sbc spiral NGC 4013, separated by ~78′ (P.A.~117°) from NGC 4051. According to de Vaucouleurs (1975), NGC 4051 is a member of Canes Venatici II Cloud whose core area measures 15°×8°.

4.4 Comparison with the Synthetic Rotation Curves of Rubin et al. (1985)

Based on their extensive observations of rotation curves (Rubin *et al.* 1980, 1982, 1985), Rubin *et al.* (1985) have derived the synthetic rotation curves for Sa, Sb, and Sc galaxies as a function of absolute magnitude M_B and fraction of isophotal radius R/R_{25}. Since NGC 4051 is classified as a Sbc spiral, we averaged the Sb and Sc synthetic rotation curves with the same absolute magnitude. Comparison is shown in Fig. 9, where the isophotal radius of NGC 4051 is taken to be $R_{25}=150''$ (RC2).

The striking feature of the diagram is that the rotation velocities of NGC 4051 are different from any of the synthetic rotation curves both in the form of rotation curve and in the absolute magnitude of galaxies. As mentioned by Rubin *et al.* (1985), the synthetic rotation curves consist of sharply rising inner part and slowly increasing or nearly flat outer part. Contrary to such a common form, the rotation velocities of NGC 4051 are gradually increasing with distance from the center up to $R/R_{25}\sim0.6$, at which the rotation velocity reaches to $V\sim200$ km s^{-1}. As mentioned in Sec. *4.3*, Fig. 7(a) of Liszt & Dickey (1995) also suggests that, outside $R/R_{25}\sim0.6$, the rotation velocity may become flat. Rubin *et al.* (1985) adopt $H_0=50$ km s^{-1} Mpc^{-1}, in which case we have $M_B=-20.2$ for the absolute magnitude of NGC 4051 (de Vaucouleurs & de Vaucouleurs 1968, RC3; Tully 1988). Then, the Sbc synthetic rotation curve with $M_B=-20.0$ gives $V=136$ km s^{-1} at $R/R_{25}=0.6$, much

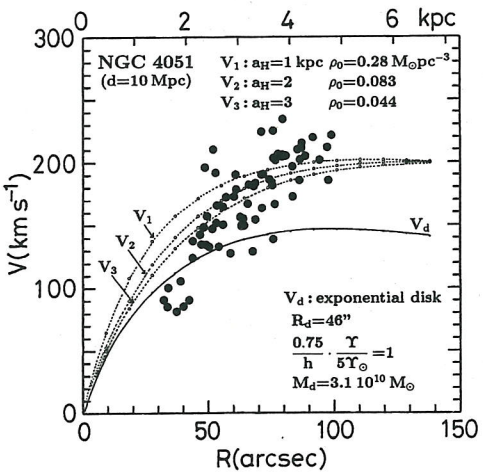

FIG. 10. Comparison with the model circular-speed curves. The model curve denoted by R_d is for an exponential disk with the disk scale length $R_d = 46''$ (2.2 kpc), the central surface brightness $\mu_B(0) = 21.4$, and the mass-to-light ratio $0.75\Upsilon/5h\Upsilon_\odot = 1$, where h is the Hubble constant in units of 100 km s^{-1} Mpc^{-1}. Three dotted curves are the composite ones of the disk and spherical dark halos with the scale parameter $a_H = 1$, 2, and 3 kpc, the central density ρ_0 being evaluated so that $V \approx 200$ km s^{-1} at $R \approx 130''-140''$. The distance $d = 10$ Mpc is assumed in calculating the velocities of the dark halo and for the upper scale.

smaller than $V \sim 200$ km s^{-1} mentioned above for NGC 4051.

One may doubt whether the assumed inclination of $i = 37°$ is wrong. However, NGC 4051 becomes nearly edge-on to reduce the velocities of NGC 4051 to the corresponding synthetic rotation curve. Such a large inclination seems inconsistent with the morphology of the galaxy.

Using multiaperture photometric data of NGC 4051 (de Vaucouleurs & de Vaucouleurs 1968; Longo & de Vaucouleurs 1983), we tentatively derived $R_d \approx 46''$ and $\mu_B(0) \approx 21.4$ for the disk scale length and central surface brightness of the exponential disk (Freeman 1970), respectively.

With the help of equation (2.169) of Binney & Tremaine (1987), these parameters enable us to calculate $V_d(R)$ the circular speed of the exponential disk. The result is shown in Fig. 10. This curve has the maximum velocity

$$V_m \approx 146 \sqrt{\frac{0.75}{h} \cdot \frac{\Upsilon}{5\Upsilon_\odot}} \text{ km s}^{-1} \quad \text{at} \quad R \approx 2.2 R_d, \qquad (5)$$

where Υ is the mass-to-light ratio, and h is the Hubble constant in units of 100 km s^{-1} Mpc^{-1}. Thus, we can confirm that the synthetic rotation curve of Sbc galaxies with $M_B = -20$ ($h = 1.0$) is consistent with $\Upsilon \sim 5\Upsilon_\odot$ appropriate for the disk of Sbc galaxies (Faber & Gallagher 1979; Binney & Tremaine 1987).

Then, a high mass-to-light ratio of $\Upsilon \sim 10h\Upsilon_\odot$ is required to explain the rotation velocities of NGC 4051 ($V \sim 200$ km s^{-1} at $R/R_{25} \sim 0.6$) in terms of the rotation of the disk. Alternatively, if the disk of NGC 4051 is normal in mass-to-light ratio as a Sbc spiral, an another source of gravity, for example, a dark halo should be taken into account for a kinematic interpretation of NGC 4051.

Adopting a distance of 10 Mpc and assuming a spherical dark halo whose density distribution (Bahcall & Soneira 1980) is given by

$$\rho(r) = \frac{\rho_0}{1 + (r/a_H)^2}, \qquad (6)$$

we tentatively computed the circular speed and the mass, where ρ_0 and a_H are the central density and core radius of the halo, respectively. It should be noticed that the total mass in the halo with the above density distribution diverges. Unfortunately, we have no knowledge concerning ρ_0 and a_H. Then, for three core radii of $a_H = 1$, 2, and 3 kpc, we tried to calculate the circular speed of the system consisting of the halo and the exponential disk described above. The value of ρ_0 was evaluated so that the circular speed of the system is 200 km s^{-1} at $R = 130''-140''$. The results are shown in Fig. 10. The mass of the halo within 10 kpc radius is estimated to be $\sim 3 \times 10^{10}$ $\mathcal{M}_\odot$ for three cases. However, we should bear in mind that, from comparison of Fig. 10, any definite constraints are not in place, because the photometric parameters used for the exponential disk are not derived directly from imaging observations.

5. CONCLUDING REMARKS

We have presented the observational data of Hα velocities for the nearest Seyfert galaxy NGC 4051. The $3' \times 3'$ region of the galaxy has been almost covered by the 17 slit positions (P.A. = 110°). The emission region is rather annular, and the observed velocities are gradually increasing with distance from the center up to $r \sim 90''$. No maximum or flat part is found in the observed rotation curve. The least-squares method gives $V_h = 697 \pm 11$ km s^{-1} and $\phi = 130° \pm 14°$ for the heliocentric systemic velocity and the major axis position angle, respectively. The velocities corrected for the galaxy inclination $i = 37°$ reach to $V \sim 200$ km s^{-1} at $R \sim 90''$.

The Hα velocity structure is consistent with the H I observations of Liszt & Dickey (1995). However, the velocity curve of NGC 4051 is quitely different from any of the synthetic rotation curves compiled by Rubin *et al.* (1985) both in the form of the rotation curve and in the absolute magnitude of galaxies. At present, we have no reasonable explanation for these disagreements.

Our comparison with the synthetic rotation curves of Rubin *et al.* (1985) is based on a rough estimation of the disk parameters R_d and $\mu_B(0)$. We suppose that those parameters should be derived from direct imaging observations. In 1996 February and 1997 March, we have obtained the deep CCD images of NGC 4051 in *BVRI* bands using the Kiso 105 cm Schmidt telescope. In a near future, we wish to report the reanalysis of the velocity structure of NGC 4051 together with the surface photometry.

We are grateful to the staff of the Okayama Astrophysical Observatory for help with the observations. We also wish to thank the anonymous referee for useful comments.

REFERENCES

Aoki, K., Ohtani, H., Yoshida, M., & Kosugi, G. 1994, PASJ, 46, 539
Aoki, K., Ohtani, H., Yoshida, M., & Kosugi, G. 1996, AJ, 111, 140
Bahcall, J. H., & Soneira, R. M. 1980, ApJS, 44, 73
Barnes, J. V., & Hayes, D. S. 1982, 1984, IRS Standard Star Manual, Kitt Peak National Observatory
Binney, J., & Tremaine, S. 1987, Galactic Dynamics (Princeton University Press, Princeton)
Bottinelli, L., Gouguenheim, L., Fouquè, P., & Paturel, G. 1990, A&AS, 82, 391
Byrd, G. G., Sundelius, B., & Valtonen, M. 1987, A&A, 171, 16
Christopoulou, P. E., Holloway, A. J., Steffen, W., Mundell, C. G., Thean, A. H. C., Goudis, C. D., Meaburn, J., & Pedlar, Ap. 1997, MNRAS, 284, 385
de Vaucouleurs, G. 1975, in Galaxies and the Universe, edited by A. Sandage, M. Sandage, and G. A. Tammann (University of Chicago Press, Chicago), p. 575
de Vaucouleurs, G., & de Vaucouleurs, A. 1968, Basic Data on Seyfert Galaxies (Pub. Department of Astronomy, The Univ. Texas at Austin, Series II, Vol. 2, No. 7)
de Vaucouleurs, G., de Vaucouleurs, A., & Corwin, H. G. 1976, Second Reference Catalogue of Bright Galaxies (University of Texas Press, Austin) (RC2)
de Vaucouleurs, G., de Vaucouleurs, A., Corwin, Jr., H. G., Buta, R., Paturel, G., & Fouqué, P. 1990, Third Reference Catalogue of Bright Galaxies (Springer, New York) (RC3)
Evans, I. N., & Dopita, M. A. 1985, ApJS, 58, 125
Evans, I. N., Koratkar, A. P., Storchi-Bergmann, T., Kirkpatrick, H., Heckman, T. M., & Wilson, A. S. 1996, ApJS, 105, 93
Faber, S. M., & Gallagher, J. S. 1979, ARA&A, 17, 135
Freeman, K. C. 1970, ApJ, 160, 811
Huchra, J., & Burg, R. 1992, ApJ, 393, 90
Kaneko, N., Satoh, T., Toyama, K., Sasaki, M., Nishimura, M., & Yamamoto, M. 1992, AJ, 103, 422
Kodaira, K., Okamura, S., & Ichikawa, S. 1990, Photometric Atlas of Northern Bright Galaxies (University of Tokyo Press, Tokyo)
Kosugi, G., *et al.* 1995, PASP, 107, 475
Kunieda, H., Hayakawa, S., Tawara, Y., Koyama, K., Tsuruta, S., & Leighly, K. 1992, ApJ, 384, 482
Lawrence, A., Watson, M. G., Pounds, K. A., & Elvis, M. 1985, MNRAS, 217, 685
Liszt, H. S., & Dickey, J. M. 1995, AJ, 110, 998
Longo, G., & de Vaucouleurs, A. 1983, A General Catalogue of Photometric Magnitudes and Colors in the U,B,V System (University of Texas, Austin)
McHardy, I. M., Green, A. R., Done, C., Puchnarewicz, E. M., Mason, K. O., Branduardi-Raymont, G., & Jones, M. H. 1995, MNRAS, 273, 549
Nilson, P. 1973, Uppsala General Catalogue of Galaxies (Uppsala)
Papadakis, I. E., & Lawrence, A. 1995, MNRAS, 272, 161
Rubin, V. C., Ford, Jr., W. K., & Thonnard, N. 1980, ApJ, 238, 471
Rubin, V. C., Ford, Jr., W. K., Thonnard, N., & Burstein, D. 1982, ApJ, 261, 439
Rubin, V. C., Burstein, D., Ford, Jr., W. K., & Thonnard, N. 1985, ApJ, 289, 81
Sandage, A., & Bedke, J. 1988, Atlas of Galaxies (NASA, Washington, DC)
Sandage, A., & Bedke, J. 1994, The Carnegie Atlas of Galaxies (Carnegie Institution of Washington, Washington, DC)
Sandage, A., & Tammann, G. A. 1981, A Revised Shapley-Ames Catalog of Bright Galaxies (Carnegie Institution of Washington, Washington, DC) (RSA)
Simkin, S. M., Su, H. J., & Schwarz, M. P. 1980, ApJ, 237, L1
Tully, R. B. 1988, Nearby Galaxies Catalog (Cambridge University Press, Cambridge)
Veilleux, S., & Osterbrock, D. E. 1987, ApJS, 63, 295
Yahil, A., Tammann, G. A., & Sandage, A. 1977, ApJ, 217, 903
Yoshida, M., Yamada, T., Kosugi G., Taniguchi, Y., & Mouri, H. 1993, PASJ, 45, 761